Study of Uniaxially Stretched Isotactic Poly(propylene) by ^{1}H Solid-State NMR and IR Spectroscopy

Cristian Hedesiu, Dan E. Demco,* Klaas Remerie, Bernhard Blümich, Victor M. Litvinov*

Changes in the amount of the rigid, semi-rigid and soft fractions, molecular mobility and domain thickness of uniaxially stretched iPP were investigated as a function of temperature, draw ratio, drawing temperature and drawing rate. Correlations are established between the thicknesses of rigid domains and the amount of the rigid fractions of uniaxially stretched iPP. Also established are correlations between the thickness of rigid domains and the molecular mobility of the rigid fraction of uniaxially stretched iPP. The drawing temperature has an important effect on the strain-induced transformation of the spherulitic morphology of iPP to a fibrillar one.

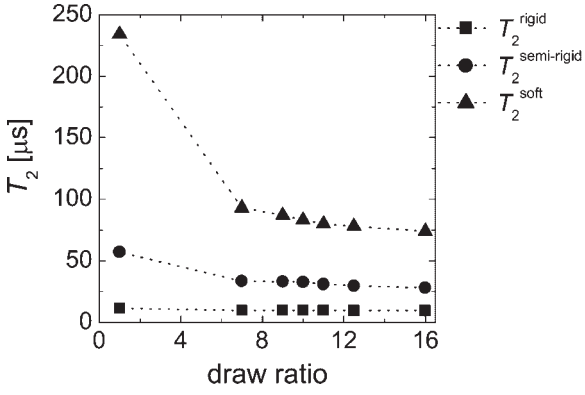

Introduction

The mechanical properties of semi-crystalline polymers are strongly affected by changes in the degree of crystallinity due to variation in the molecular structure, different processing conditions of polymeric articles and loading conditions.[1–11] Loading conditions include the drawing temperature, draw ratio and the strain rate.[12–14] The deformation process of semi-crystalline polymers has been extensively investigated using a variety of methods for many years.[15–21] When the semi-crystalline polymers are highly drawn, the shear forces destroy the spherulites. This is followed by the reorganization of the spherulitic morphology to another type of morphology, depending on the material drawn and the drawing conditions. Several modes of deformation above the glass transition temperature have been identified in semi-crystalline polymers. According to Flory and Yoon,[22] plastic deformation occurs by partial melting and re-crystallization of the crystalline phase. However, according to Peterlin,[23] the plastic deformation during the application of stress occurs in three stages. In the first stage, the plastic deformation of the original spherulitic structure occurs. The deformation occurs by strain of the interlamellar soft regions with a combination of interlamellar separation, lamellae stack rotation, interlamellar shear deformation and

C. Hedesiu, B. Blümich
Institut für Technische Chemie und Makromolekulare Chemie, Rheinisch-Westfälische Technische Hochschule, Worringer Weg 1, D-52056 Aachen, Germany
C. Hedesiu, V. M. Litvinov
DSM Research, Resolve, P. O. Box 18, 6160 MD Geleen, The Netherlands
E-mail: victor.litvinov@dsm.com
D E. Demco
Deutsches Wollforschungsinstitut an der RWTH, Pauwelstrasse 1, D-52074 Aachen, Germany
E-mail: demco@mc.rwth-aachen.de
K. Remerie
SABIC Europe BV, P. O. Box 319 6160 AH, Geleen, The Netherlands

Macromol. Chem. Phys. **2008**, *209*, 734–745

DOI: 10.1002/macp.200700503

cavitation.[24–26] In the second stage, the discontinuous transformation of the spherulitic structure in the fibrillar morphology takes place. During this stage, the lamellae in the microneck are fragmented and the broken crystal blocks are incorporated into the newly formed microfibrils. In uniaxial drawing, the blocks are not only moved in the draw direction, but also in the direction perpendicular to it.[27] The chains connecting the broken crystal blocks in the lamellae serve as intramicrofibrillar tie molecules. In the third stage, the plastic deformation of the fibrillar structure occurs. The drawing of the microfibrillar structure[28] is completely different from the initial plastic deformation that transforms the lamellae into the microfibrillar morphology. The thickness of the fibrils changes almost proportionally to the draw ratio, as a consequence of the much smaller shear displacement of the constituting microfibrils, caused by the shear stress on the fibrils.[29]

The crystallinity, molecular mobility, lamellar thickness and structural orientation in both soft and crystalline phases are important parameters regarding the physical and mechanical properties of stretched and non-stretched iPP. There are several methods for the structural characterization of soft and crystalline phases of the polymers. One of the methods, solid-state NMR, is capable of characterizing the crystallinity, the molecular mobility, domain thicknesses and phase-selective characterization of the orientation distribution function of semi-crystalline polymers.[30–38] Another method is IR spectroscopy, which can be used to determine the degree of crystallinity of iPP.[39–41] Knowledge of strain-induced order in the crystalline and soft phases of stretched iPP under various conditions is valuable information for understanding the structure reorganization mechanisms, and their relation to the mechanical properties of iPP.

Wide-angle X-ray diffraction (WAXD) provides information about the crystal lattice order, strain-induced changes in the orientation of crystalline domains and highly oriented crystalline structures in the fibrillar morphology generated in the neck part of uniaxially stretched polymers.[42] Very little information about strain-induced changes in the soft component can be obtained from WAXS. Small angle X-ray scattering (SAXS) provides information about lamella packing, orientation and long period.[43–47]

The infrared (IR) spectroscopy and NMR evidence for structural reorganization during deformation is rather indirect as far as morphology is concerned. Transmission electron microscopy (TEM) yields direct access to the details of the lamellar morphology.[48,49] It is thought that IR and NMR are complementary techniques providing morphological evidence on nanometer scale phenomena for stretched iPP, the phase composition, molecular mobility and the orientation. In a recent investigation of iPP by NMR, SAXS, WAXD, DSC and TEM,[52] the phase composition, chain mobility and domain thicknesses were correlated.

The focus of this paper is to study the change in the phase composition/crystallinity, molecular mobility and lamellae thicknesses in iPP upon uniaxial drawing at different drawing temperatures and rates. Two complementary methods, ^{1}H solid-state NMR and IR, were used in the present study. The study largely focuses on strain-induced changes in the soft phase that have not been analyzed previously in detail.

Experimental Part

Sample Description and Preparation

The isotactic poly(propylene) (iPP-PP575P) homopolymer samples used in the present study were manufactured by SABIC Europe BV. The stereochemical defects were in the range of 1%. The material was characterized by a melt flow index of 10 g·10 min^{-1}. The material was injection-molded using an Engel 45A machine into plates of 12×12 cm^2 and 4 mm thickness. The melt temperature was set to 235 °C, the holding pressure was 40 MPa, and the holding, cooling and overall cycle time were 20, 20 and 49.5 s, respectively.

Dog bone shaped tensile bars with a length of 70 mm, thickness of 4 mm and gauge dimensions of 20 mm length were cut from the injection molded iPP plates. The samples were uniaxially stretched at different temperatures (25, 80 and 110 °C) and different rates (1, 10, 50 and 100 mm·min^{-1}) to draw ratios in the range of $\lambda = 7$–16 using a Zwick Z050 tensile machine. New tensile bars were used for each NMR experiment as a function of temperature, strain and deformation rate. Based on literature information,[23] we assumed that in this deformation range the spherulitic structure is transformed into a fibrillar structure. Since no homogeneous neck formation was observed at $\lambda = 1$–6, samples in this range of strain were not studied. All the NMR and IR experiments in this study were performed on the neck part of stretched samples after 2 h of strain recovery. The temperature for the NMR measurements was 70 °C, different from the drawing temperatures. The changes in the draw ratio at the end of NMR measurements were of the order of 10–20%. This implies that from the present study no conclusion can be drawn regarding chain mobility and phase content during deformation, but exclusively we can conclude on the post mortem status (i.e., after elastic recovery). The neck of the tensile bars was cut into small pieces that were positioned in a quasi-isotropic distribution inside a 10 mm NMR tube.

IR Measurements

IR experiments were performed on a Perkin Elmer AutoImage FTIR microscope. IR spectra (4 000–6 000 cm^{-1}) were acquired at a spectral resolution of 4 cm^{-1}, using 200 accumulations. Three spectra were acquired for each sample, namely without polarization, with IR light polarized parallel to the drawing direction of the

polymer and with IR light polarized perpendicular to the drawing direction of the polymer. Dichroic analyses were carried out using a wire grid polarizer. The sample was rotated rather than the polarizer, as it was known that the exciting beam of the used spectrometer is partly polarized. The data processing procedure followed the method provided by Kissin.[41]

NMR Measurements and Data Analysis

Transverse Magnetization Relaxation (T_2) Measurements

Proton NMR transverse magnetization relaxation (T_2) experiments were carried out in order to study the phase composition and molecular mobility in both non-stretched and uniaxially stretched iPP. The experiments were performed in a low static magnetic field using a Bruker MQ20 minispec spectrometer operating at a proton frequency of 19.65 MHz. The duration of the 90 ° pulse excitation was 2.6–2.7 μs, the dead time was 7 μs and the dwell time was 0.5 μs. The data were collected at temperatures between 25 and 140 °C. Measurements as a function of increasing temperature were performed 10 min after thermal stabilization at each temperature. Measurement times at each temperature were approximately 2 h. Two different NMR pulse sequences were used to measure the decay of the ^{1}H transverse magnetization (T_2 relaxation), from the rigid, semi-rigid and soft fractions of the sample. In the first experiment, the free induction decay (FID) was recorded after a 90° pulse excitation (SPE, single pulse excitation), i.e., 90°_x – dead time – acquisition of the amplitude $A(t)$ of the transverse magnetization as a function of time t. The second experiment was the Hahn echo pulse sequence (HEPS), i.e., 90°_x–t_{HE}–180°_y–t_{HE}–acquisition of the amplitude of the echo maximum for variable values of $2t_{HE}$.[50]

The results obtained from both SPE and HEPS experiments were combined in a single decay (Figure 1), which was fitted with a linear combination of one Abragam function and two exponential functions (Equation (1)):

$$A(t) = A(0)^{\text{rigid}} \exp\left[-\left(\frac{t}{T_2^{\text{rigid}}}\right)^2\right] \cdot \left(\frac{\sin at}{at}\right) + A(0)^{\text{semi-rigid}} \exp\left(-\frac{t}{T_2^{\text{semi-rigid}}}\right) + A(0)^{\text{soft}} \exp\left(-\frac{t}{T_2^{\text{soft}}}\right) \quad (1)$$

The parameter a of the Abragam function is related to the second and fourth van Vleck moments.[51] The transverse relaxation times (T_2), which are characteristic of different slopes in the magnetization decay curve, are related to molecular mobility in each fraction. The relative fraction of the k-relaxation components, $\{A(0)^k/[A(0)^{\text{rigid}} + A(0)^{\text{semi-rigid}} + A(0)^{\text{soft}}]\} \times 100\%$, represents the relative amount of hydrogen atoms (mass fractions) of iPP phases/fractions with different molecular mobility. Repeated experiments indicated that the relative error of the relaxation parameters was about 1%.

Spin Diffusion Experiments with Double Quantum Dipolar Filter

Spin diffusion experiments with a double quantum (DQ) dipolar filter were performed in order to determine the thickness of rigid and soft domains of both non-stretched and uniaxially stretched iPP. In the present work, ^{1}H spin-diffusion data were recorded in a low magnetic field at 70 °C using a Bruker Minispec MQ20. Spin diffusion experiments were performed using the pulse sequence $90^\circ_x - \tau - 90^\circ_{-x} - t_{DQ} - 90^\circ_y - \tau - 90^\circ_{-y} - t_d - 90^\circ_x$ – FID with an excitation/reconversion time τ of 10 μs and the spin-diffusion time, t_d. The evolution time of the DQ coherences (t_{DQ}) was 5 μs in all experiments. All the experimental details concerning the spin-diffusion experiments and data analysis have been described previously.[50]

No correction of the spin-diffusion data due to a longitudinal relaxation T_1 effect was performed, because the spin-diffusion process was nearly completed at the longest mixing time of 16 ms. This time is significantly shorter than T_1 for all studied samples.

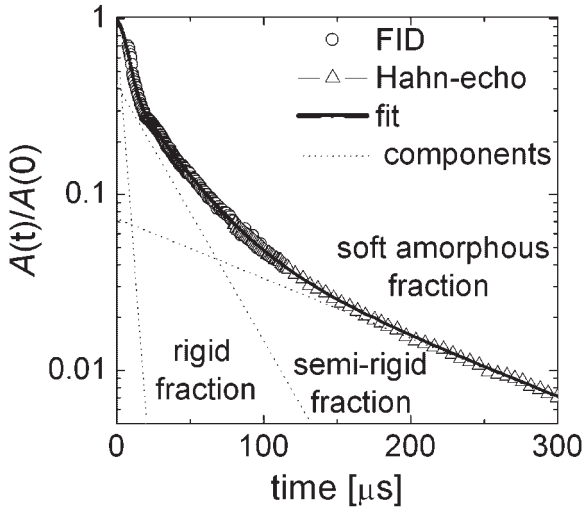

Figure 1. The decay of the ^{1}H transverse magnetization relaxation at 70 °C for uniaxial iPP stretched at 80 °C with a draw rate of 10 mm · min^{-1} and with a draw ratio of $\lambda = 10$. The decay (FID) was measured at 19.65 MHz using the SPE (○) and the HEPS (△) methods. The solid line represents the result of a least-squares fit of the decay with a linear combination of the Abragam function and two exponential functions. Dotted lines show the separate components that are assigned to rigid, semi-rigid and soft fractions of stretched iPP.

Results and Discussion

Stress-Strain Characteristics

Figure 2(a) shows the stress-strain curves for stretched iPP samples that were uniaxially stretched at a deformation rate of 10 mm · min^{-1} in a temperature range between 25 and 110 °C. It can be observed that the deformation

Macromol. Chem. Phys. **2008**, *209*, 734–745

Macromolecular Journals

DOI: 10.1002/macp.200700503

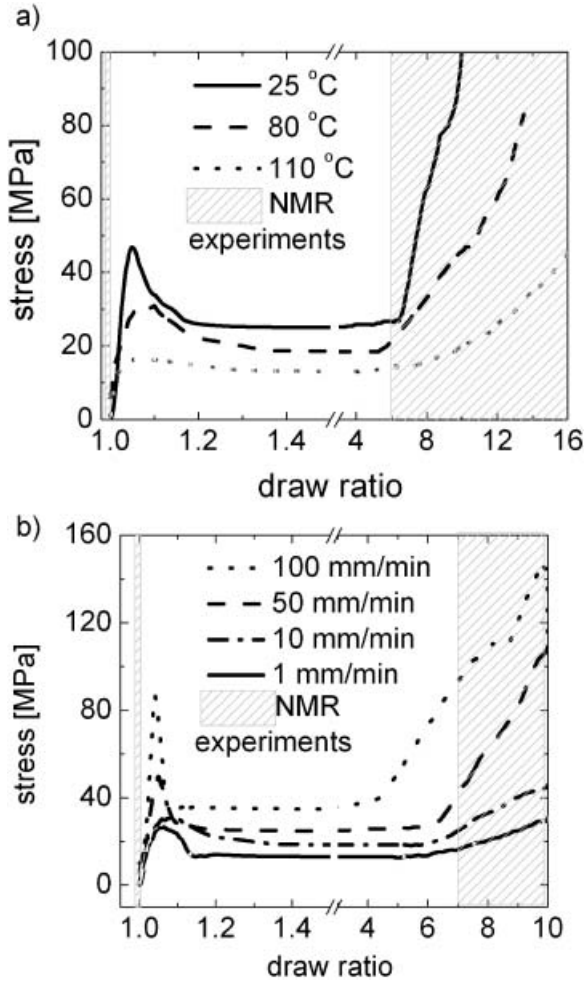

Figure 2. Stress-strain curve recorded (a) at 25, 80 and 110 °C under a constant drawing rate of 10 mm · min^{-1}, and (b) with different drawing rates of 1, 10, 50 and 100 mm · min^{-1} at 80 °C. The hashed area corresponds to the draw ratio λ when the NMR experiments were performed for the recovery after strain sample.

behavior of iPP is strongly affected by the temperature. For the drawing temperature range between 25 and 110 °C, typical ductile deformation behavior with a yield point, neck formation and propagation, and strain hardening is found. In the low temperature region, a pronounced yield point occurs, which is related to necking and the inhomogeneous deformation of the iPP samples. At a microscopic scale, this corresponds to the beginning of the transformation of the initial spherulitic morphology into a fibrillar morphology. The higher values of the yield stress at low drawing temperatures can be explained with an increasingly important contribution from the soft phase to strain-induced changes in the crystalline phase due to the low chain mobility in the soft phase. With increasing drawing temperature, the yield stress and strain hardening decrease. The strain-hardening region also becomes less well defined and the yield point becomes diffuse. At high drawing temperatures, the increase in the chain mobility of iPP chains in the soft and crystalline regions (see below) results in a lower stress required for strain-induced morphological changes. Strain hardening is related to an increase in stress when the neck propagation over the whole length of the gauge part of the sample is achieved. The onset strain hardening seems to be slightly shifted to a higher draw ratio with increasing temperature. Figure 2(b) shows the stress-strain curves of stretched iPP samples at 80 °C with different drawing rates of 1, 10, 50 and 100 mm · min^{-1}. The yield stress and strain hardening both increase with increasing strain rate at 80 °C (see Figure 2(b)). These changes indicate that chain mobility plays an important role in the molecular rearrangements that are required for strain-induced morphological changes. Chain motions recover after strain samples cause strain release. Therefore, strain increases with the deformation rate.

Crystallinity by IR

Infrared analyses were carried out on three samples, namely $\lambda = 7$, 10 and 12.5. The samples were deformed at 80 °C with 10 mm · min^{-1}. Dichroic and non-polarized spectra of one of the samples ($\lambda = 10$) are provided in Figure 3. It is clear that orientation of the sample has a distinct effect on the acquired spectra, indicating that the sample is not isotropic. Peak heights of the relevant peaks were extracted from these spectra based on the definitions mentioned in the Experimental Part,[41] and used to calculate the crystallinity (c.f. Table 1). Due to the experimental errors we cannot draw a conclusion about the dependency of the crystallinity as a function of draw ratio, however it is clear that the value of rigid fraction

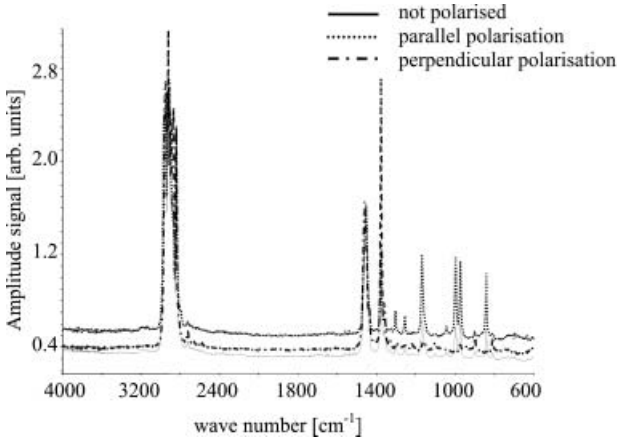

Figure 3. Polarized and non-polarized IR spectra of the stretched iPP at 80 °C and $\lambda = 10$. The drawing rate was 10 mm · min^{-1}.

Table 1. Crystallinity of uniaxially stretched iPP determined by IR spectroscopy using the Kissin method.[41] The samples were uniaxially drawn at 80 °C at 10 mm · min^{-1}.

Sample	Crystallinity[a)]
$\lambda = 7$	67
$\lambda = 10$	66
$\lambda = 12.5$	69

[a)]The errors are of the order of 10%.

from NMR is in the same order of magnitude as crystallinity measured by IR.

Proton Solid-State NMR Study of the Phase Composition, Chain Mobility and Thickness of Domains of Uniaxially Stretched iPP

Temperature Dependence of the Phase Composition and Chain Mobility for a Uniaxially Stretched iPP Sample

The temperature dependence of the amount of the rigid, semi-rigid and soft fractions for both non-stretched and uniaxially stretched iPP samples at 80 °C, and at three different drawing ratios ($\lambda = 1$, 7 and 12.5), at a drawing rate of 10 mm · min^{-1} are shown in Figure 4(a). For the non-stretched iPP sample ($\lambda = 1$), the content of the rigid fraction first decreases upon heating to 60 °C, then it is almost constant in the temperature range from 60 to 110 °C, and finally decreases from 120 °C onwards due to partial melting. In the temperature range from 40 to 60 °C, a significant fraction of the soft phase is immobilized and contributes to the amount of detected rigid fraction (see Figure 4(a)). In this temperature range, the amount of rigid fraction is composed of the crystalline phase and immobilized fraction of the soft phase. The amount of the soft fraction increases upon increasing the temperature. This increase is accompanied by an increase in molecular mobility of the less constrained chain fragments in the soft phase as it follows from T_2^{soft} (see Figure 4(b)). In the temperature range from approximately 60 to 100 °C, the amount of the rigid fraction is close to the crystallinity determined by SAXS and DSC.[50] Above 110 °C, the amount of the rigid fraction of iPP decreases due to the partial melting of thin lamellae. The iPP samples, having recovered after strain, show a similar temperature dependence of the amount of each fraction as non-deformed iPP samples.

Thus, above 40 °C, three different fractions (Figure 4(a)) with different mobilities (Figure 4(b)) are detected. The characteristic decay time, T_2, is related to the chain mobility in different fractions. The relaxation time of the rigid fraction (T_2^{rigid}) in all the samples slightly increases upon temperature. The small increases in T_2^{rigid} with

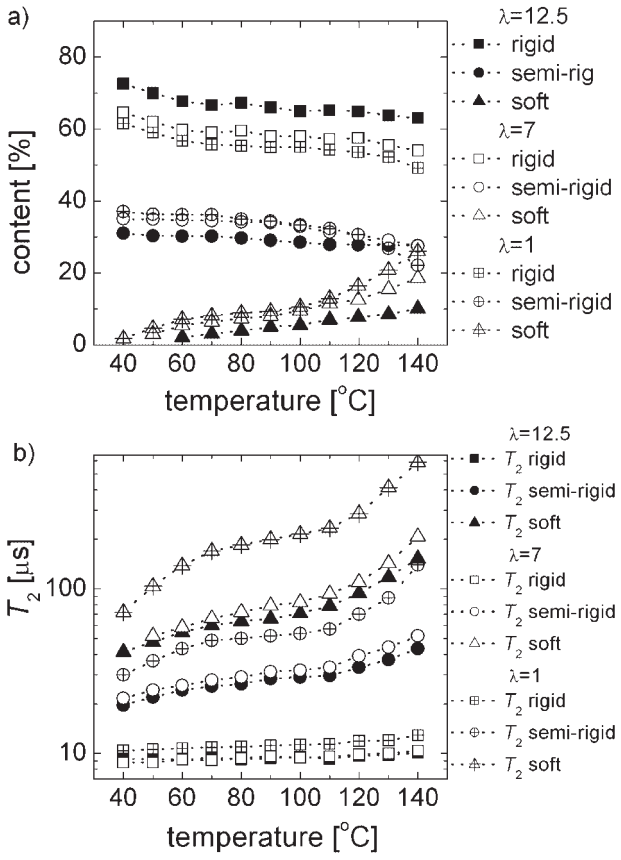

Figure 4. (a) Temperature dependence of the amounts of rigid, semi-rigid and soft fractions of non-stretched iPP ($\lambda = 1$) and uniaxially stretched iPP ($\lambda = 7$ and 12.5). The samples were stretched at 80 °C with a draw rate of 10 mm · min^{-1}. (b) Temperature dependence of the ^{1}H T_2 relaxation times (T_2^{rigid}, $T_2^{semi-rigid}$ and T_2^{soft}) for both non-stretched and uniaxially stretched iPP samples. The NMR experiments were performed at 70 °C.

increasing the temperature could be related to the α_c relaxation process.[31] The intermediate $T_2^{semi-rigid}$ relaxation time increases with increasing the temperature, but its value does not largely exceed T_2^{rigid} for the same sample at a given temperature. This indicates that the segmental motion responsible for $T_2^{semi-rigid}$ is largely restricted. A significant difference in temperature dependence for the sample with different draw ratios is observed for the relaxation time of the soft fraction T_2^{soft} (Figure 4(b)). With increasing draw ratio, the constraints on the segmental mobility in both soft and semi-rigid component slowly increase. This leads to a decrease of $T_2^{semi-rigid}$ and T_2^{soft}, which is especially in the strain-hardening region ($\lambda \approx 7$) of the samples.

The Effect of Draw Ratio on the Phase Composition and Molecular Mobility

In order to study the structural changes caused by drawing, the amount of rigid, semi-rigid and soft fractions

Macromol. Chem. Phys. **2008**, *209*, 734–745

Macromolecular Journals

DOI: 10.1002/macp.200700503

that was measured at 70 °C is plotted as a function of draw ratio for iPP samples which were uniaxially stretched at 80 °C, with a drawing rate of 10 mm · min^{-1} (Figure 5(a)). Drawing to $\lambda = 7$ caused a small increase in the amount of the rigid fraction, which indicates the presence of highly strained tie molecules. On increasing the draw ratio to 10–16, a further increase in the amount of the rigid fraction is observed. This increase can be attributed to strain-induced crystallization due to the high straining of chain in the soft component and/or large immobilization of chains in the soft phase due to their elongation. In the deformation range from $\lambda = 7$ to 12.5 the amount of the rigid fraction is in good correspondence with the degree of crystallinity obtained by IR (see Figure 5(a)). Thus, the increase in the amount of the rigid fraction seems to be mainly due to strain-induced crystallization.

In order to reveal the effect of drawing on the mobility of the rigid, semi-rigid and soft fractions, T_2^{rigid}, $T_2^{semi-rigid}$ and T_2^{soft} are shown as a function of draw ratio in Figure 5(b). At $\lambda = 7$, both $T_2^{semi-rigid}$ and T_2^{soft} are significantly shorter than for non-stretched iPP, indicating that the molecular mobility of the semi-rigid and soft fraction largely decreases upon drawing. At $\lambda > 7$, $T_2^{semi-rigid}$ and T_2^{soft} continuously decreases up to the highest draw ratio ($\lambda = 16$). The semi-rigid fraction is not affected any more by deformation and the structural changes of the soft phase continue. All these results regarding mobility considerations have important implications for the understanding of the deformation mechanism, and the characteristic changes of the tensile modulus with draw ratio, in terms of the corresponding change in the morphology.

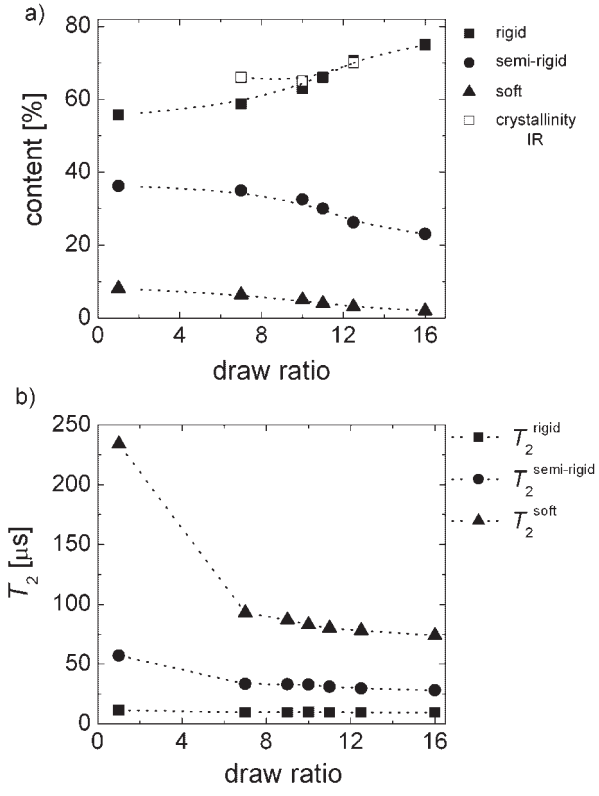

Figure 5. (a) Dependence of the amounts of rigid, semi-rigid and soft fractions at 70 °C on the draw ratio of uniaxially stretched iPP at 80 °C ($\lambda = 7$–16). The drawing rate was 10 mm · min^{-1}. The amount of the rigid fraction (■) determined by NMR at 70 °C is compared with the degree of crystallinity (□) determined by IR. (b) Draw ratio dependence of the ^{1}H T_2 relaxation times for both non-stretched and stretched iPP samples. The assignment of the T_2 value to the rigid, semi-rigid, and soft fractions of iPP is shown in the figure.

The Effect of Drawing Rate on the Phase Composition and Chain Mobility

The effect of the drawing rate on the phase composition and molecular mobility was investigated for iPP samples uniaxially stretched at 80 °C to a draw ratio $\lambda = 10$ with a drawing rate dλ/dt of 1, 10, 50 and 100 mm · min^{-1}. The NMR experiments were performed at 70 °C. The amount of the rigid, semi-rigid and soft fractions and the chain

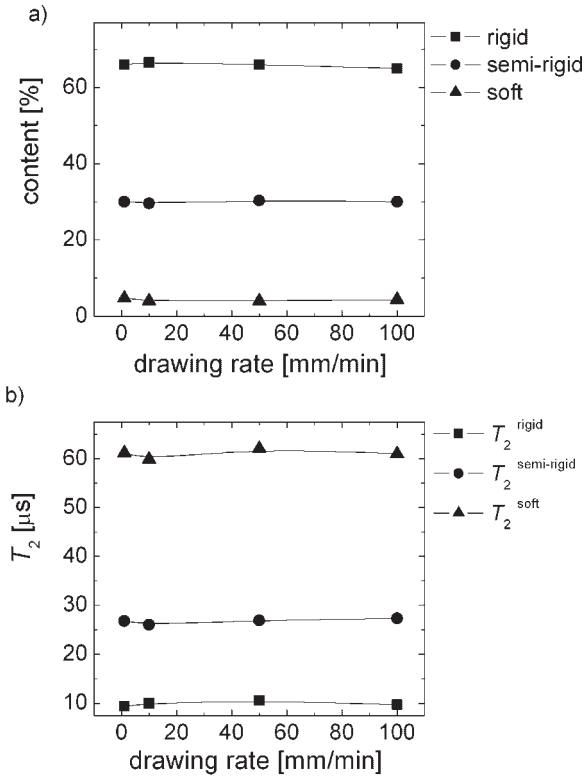

Figure 6. (a) Dependence of the amount of rigid, semi-rigid and soft fractions on the drawing rate of uniaxially stretched iPP at 80 °C and $\lambda = 10$. (b) Proton T_2 relaxation times for uniaxially stretched iPP samples as a function of drawing rate. The NMR experiments were performed at 70 °C. The lines are a guide for the eye.

mobility in each fraction of uniaxially stretched iPP is hardly affected by drawing rate, within the limit of the experimental errors (Figure 6(a) and 6(b)). These results show that the changes in the morphology and chain rearrangements upon uniaxial drawing of iPP are fast compared to the total time scale of deformation used. Another explanation could be the relaxation process which occurs when removing the sample from the tensile machine.

The Effect of Drawing Temperature on the Phase Composition and Chain Mobility

Isotactic poly(propylene) samples uniaxially stretched with a drawing rate $d\lambda/dt$ of 10 mm · min^{-1} show differences in the phase composition and chain mobility depending on the drawing temperature. All the NMR experiments were performed at 70 °C. In Figure 7(a) and 7(b), the T_2 relaxation times and the amount of the rigid, semi-rigid and soft fractions are shown as a function of both drawing temperature and drawing ratio. The amount of the rigid fraction increases when increasing the drawing temperature for all draw ratios, at the expense of both the semi-rigid and soft fractions. Chain mobility in all fractions is lower at higher deformation temperatures. The observed changes suggest that the α-relaxation influences morphological transformations via shearing and fragmentation of the lamellae upon deformation. Relative differences in imperfections in the crystalline structure can be identified by comparing the relaxation time T_2^{rigid}. Its value is longer at lower deformation temperatures at the same draw ratio λ. This indicates larger imperfections in the crystalline phase of iPP stretched at 25 °C, compared to the undeformed sample (Figure 7(b)). A small increase in the amount of the rigid fraction is observed at strain hardening deformation ($\lambda > 7$), which could be due to a large extension of the tie chains. These obtained results suggest that, at higher deformation temperatures, higher strain-induced chain orientation and better ordered crystalline structures are formed upon deformation. This is because higher chain mobility facilitates the morphological transformations, and possibly the partial melting and strain-induced crystallization occurring at higher temperatures. NMR measurements reveal that the drawing temperature has an important influence on the phase composition and molecular mobility of drawn iPP.

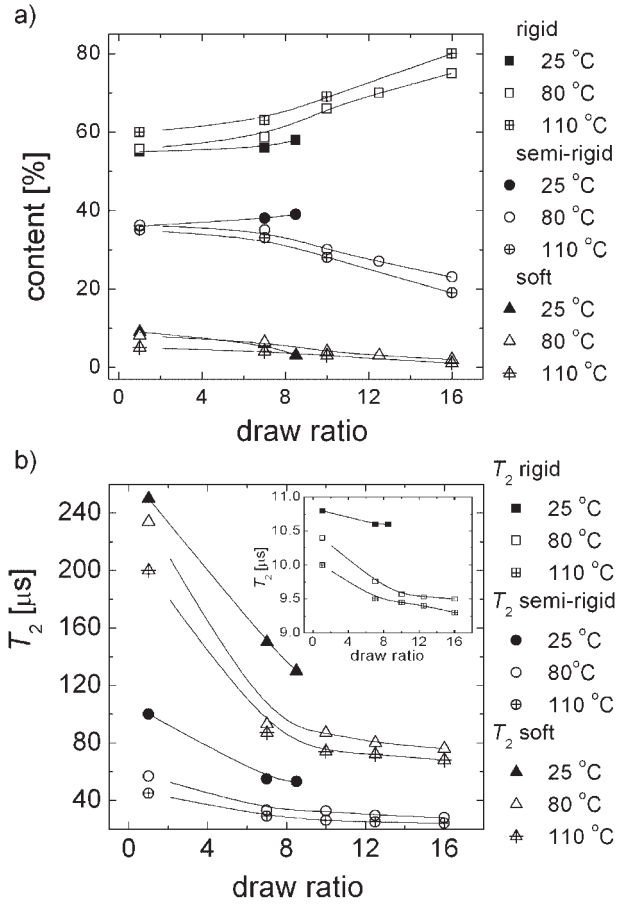

Figure 7. (a) Dependence of the amounts of rigid, semi-rigid and soft fractions on drawing temperature and draw ratios for iPP uniaxially drawn at 25, 80 and 110 °C. A draw rate of 10 mm · min^{-1} was used. The NMR measurements were performed at 70 °C. (b) Dependence of the ^{1}H T_2 relaxation times on drawing temperature and draw ratio for uniaxially stretched iPP at different temperatures. The lines are a guide for the eye.

The Effect of Draw Ratio and Drawing Temperature on Domain Sizes of iPP

The long period L_p and the thickness of the rigid d_r and semi-rigid + soft (d_{srs}) domains were studied as a function of both draw ratio and drawing temperature. The values of L_p, d_r and d_{srs} were determined from the analysis of the spin-diffusion data (measured at 70 °C) (Figure 8) with the 1D (non-stretched iPP) and 2D (stretched iPP) spin-diffusion models.[52] The different models are required because above yield strain, the spherulitic morphology is transformed into the fibrillar morphology typical for polymeric fibers. The chosen dimensionality of the spin diffusion process is established based on morphology for non-stretched and stretched polyolefins.[31,53,54] It is also confirmed by analysis that was outlined in our previous paper describing the morphology of non-stretched iPP,[52] which showed that the dimensionality of the spin-diffusion process is 1D and 2D for the initial samples and uniaxially drawn iPP, respectively. The thickness of rigid and semi-rigid + soft domains is determined for uniaxially stretched iPP because the small amount of the soft fraction, ≈2–5 wt.-% (Figure 5(a)), does not allow accurate determination of the thickness of this fraction. The estimation of the spin diffusivities was discussed at

Macromol. Chem. Phys. **2008**, *209*, 734–745

Macromolecular Journals
DOI: 10.1002/macp.200700503

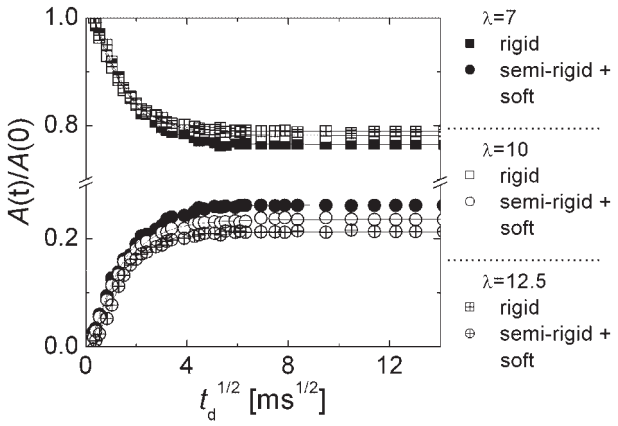

Figure 8. Proton spin-diffusion decay and build-up curves for the rigid and semi-rigid fractions of uniaxially stretched iPP to $\lambda = 7$, 10 and 12.5. Drawing temperature and drawing rate were 80 °C and 10 mm · min^{-1}, respectively. The NMR experiments were performed at 70 °C. The DQ filter selects the magnetization of the rigid fractions of stretched iPP, as described in ref.[52]. All experiments were performed on Minispec. The FID was fitted with the sum of one Abragam function and one exponential function. The solid lines represent the best fit to the 2D solutions of the spin-diffusion data for the two phase morphology.

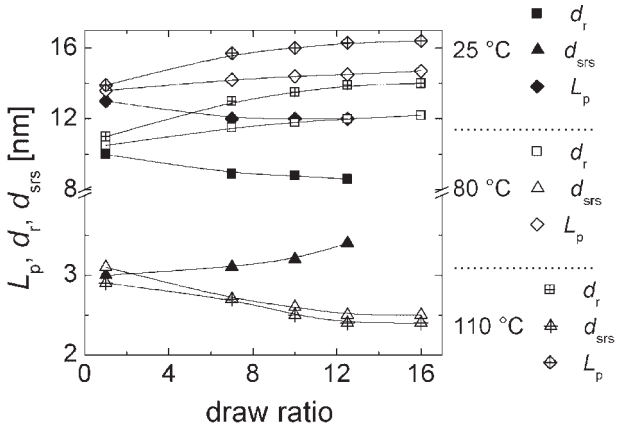

Figure 9. Dependence of long period (L_p), the thickness of the rigid (d_r) and semi-rigid + soft (d_{srs}) domains on drawing temperature and draw ratio for iPP stretched to $\lambda = 7$, 10–16 at 25, 80 and 110 °C at 10 mm · min^{-1}.

length for iPP in Ref.[52]. The fibril morphology of stretched iPP will change the spin diffusivities mainly for the rigid fraction. Because the spin diffusivity depends on the orientation relative to the static magnetic field, an average value has to be considered for the quasi-isotropic sample. This was taken into account by the evaluation of the rigid and mobile domains spin diffusivities using the effective transverse relaxation rates shown in Figure 4–7 and the theoretical consideration discussed in ref.[52].

The long period and the domain thicknesses obtained by analysis of the spin-diffusion data shown in Figure 8 are given in Figure 9. This figure shows the changes of L_p, d_r and d_{srr} upon uniaxial drawing to different draw ratios and at different drawing temperatures. At drawing temperature of 25 °C, that is below the α-relaxation temperature, the long period and the thickness of the rigid domains slightly decreases at the expense of the thickness of the semi-rigid plus soft domains (Figure 9). These dependences of the rigid domain thickness d_r and long period L_p on the deformation temperature can be explained by breakage and disordering of crystals. During the uniaxial deformation of iPP at 25 °C, the probability of the broken crystals to recrystallize and form thicker crystals is small. Strain-induced immobilization of the soft phase hinders the displacements of chains in the soft and crystalline phases that are required for lamellar thickening. No significant strain-induced crystallization and/or annealing occurs during deformation at 25 °C. At higher deformation temperatures, faster chain mobility (Figure 4) can provide the required energy to facilitate a reorganization of chains, resulting in an increase in the amount of the rigid fraction (Figure 7). For higher drawing temperatures (80 and 110 °C), an increase in the long period and thickness of lamellae is observed upon increasing the draw ratio and drawing temperature (Figure 9). The thickness of the semi-rigid plus soft layer (d_{srs}) slightly decreases with increasing the draw ratio and drawing temperature, suggesting that the crystal thickening is caused by the chain reorganization in the soft phase adjacent to the crystal surface and annealing process.

Thus, deformation at temperatures above 60 °C causes an increase in crystal thickness and long period, while deformation at lower temperatures causes a slight decrease in crystal thickness and possibly long period. The main difference between deformation at high and low temperatures is attributed to the rate of molecular motion with respect to the rate of molecular displacement with increasing strain.

Correlation between the Amount of the Rigid Fraction and the Thickness of the Crystalline Domains

Figure 10 shows the correlations between the amount of the rigid fraction and the domain thickness d_r of the rigid phase for all uniaxially stretched iPP samples at different temperatures. For the limited drawing temperature range 80–110 °C, the dependency of the amount of the rigid fraction on d_r is described by an apparently linear dependence.

The behavior of the long period presented in Figure 11 is in qualitative agreement with those reported in Ref.[55]. As proved by SAXS[55] for poly(propylene), drawing at temperatures higher than 60 °C yields an increase of long

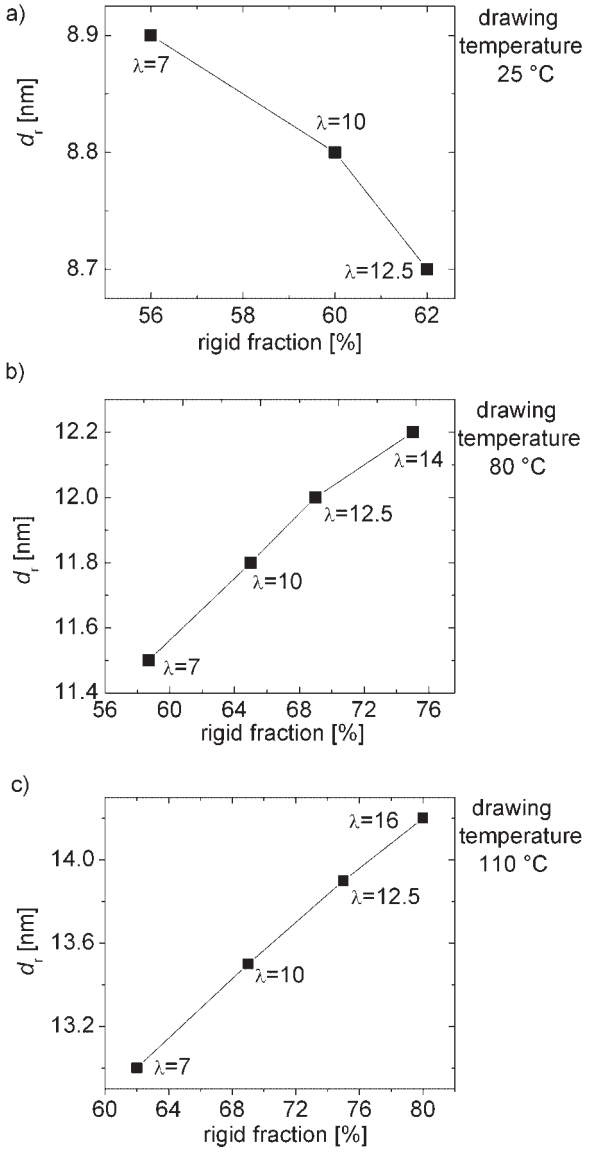

Figure 10. Correlation of the thickness of the rigid domains with the amount of the rigid fraction/crystallinity for uniaxially drawn iPP at 25 (a), 80 (b) and 110 °C (c) at 10 mm · min^{-1}.

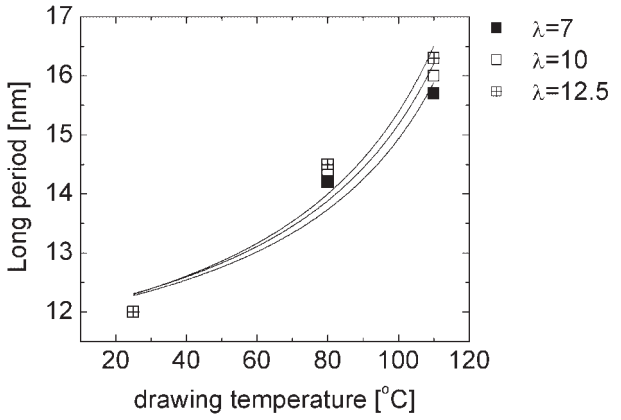

Figure 11. The long period of uniaxially drawn iPP samples at 10 mm · min^{-1} measured by ^{1}H spin-diffusion NMR as a function of drawing temperatures for different values of draw ratios. The solid lines represent the fit of the data with Equation (2). The fit parameters A and B are reported in Table 2.

period whereas deformation below these temperatures causes a decrease of the long period. This is evident from Figure 10(a–c), respectively. Nevertheless, in our case, the correlation is established between the thickness of the rigid fraction d_r and the content of the rigid fraction measured by ^{1}H spin diffusion at different drawing temperatures and draw ratios.

We shall consider in the following a semi-quantitative model to establish the correlation between the thickness of the rigid fraction d_r and the content of the rigid fraction (C_r) in the high drawing temperature regime (Figure 10(b) and 10(c)). The changes produced by deformation in polymer morphology are enhanced at higher drawing temperatures. This is due to the large mobility of polymer chains at the interface and in the soft fraction. Hence, the rigid fraction thickness and content will increase at higher drawing temperatures. In such conditions, the original morphological structure is completely destroyed and every single lamella is broken up into small folded chain blocks. The blocks are then incorporated in long microfibrils. We assume that the spin diffusion process in these microfibrils can be described by a 2D morphology as proposed for polyethylene in ref.[53]. In the approximation of a square section of microfibrils of size d_r and length h_r, the volume is $V_{\text{rigid}}^{\text{microfibril}} \approx d_r^2 h_r$. The total volume of the rigid fraction at the end of the drawing process is $V_{\text{rigid}} = N_{\text{microfiblils}} V_{\text{rigid}}^{\text{microfibril}} \approx N_{\text{microfiblils}} d_r^2 h_r$. Therefore the rigid fraction content is $C_r \propto V_{\text{rigid}}$, and finally $C_r \propto d_r^2$ or $d_r \propto (C_r)^{1/2}$. These simple arguments explain semi-quantitatively the correlation between d_r and C_r (Figure 10(b) and 10(c)). Apparently a linear dependence is shown by the data, which we believe is due to the limited range of C_r explored in the experiments. Finally, we shall point out that NMR measurements that establish the rigid domain thickness and phase composition are independent.

Correlation between the Long Period and the Drawing Temperatures

The long period (L_p) was measured for different iPP samples drawn at different draw ratios $\lambda = 7$–16 in the temperature (T_d) range from 25 °C to 110 °C using a ^{1}H spin-diffusion method. Our particular interest is the influence of the drawing temperature on the long period (Figure 11). The long period first increases rather slowly with temperature and finally increases rapidly near the melting point. Such investigation was reported before on polyethylene.[55–57]

Macromol. Chem. Phys. **2008**, *209*, 734–745

Macromolecular Journals
DOI: 10.1002/macp.200700503

Table 2. The values of the constants A and B from Equation (2) obtain from the fit of the data shown in Figure 11.

Draw ratio	A	B
	nm	nm T
7	9.7 ± 0.8	355.1 ± 69.9
10	9.5 ± 0.9	383.7 ± 77.6
12.5	9.3 ± 0.9	413.2 ± 74.5

The long period of drawn iPP as a function of drawing temperature is shown in Figure 11. This dependence can be represented approximately[55–57] by Equation (2):

$$L_p = A + \frac{B}{T_m^0 - T_d} \quad (2)$$

where T_m^0 is very close to the melting temperature ($T_m = 160\,^\circ C$) and T_d is the temperature of drawing. The continuous lines in Figure 11 represents the fit of the data with Equation (2). The constants A and B are given in Table 2 for different draw ratios. They are in the same range of values as those reported for polyethylene.[56,57] The long period were measured in this case by SAXS. These results prove indirectly that the spin-diffusion measurements give valid trend for the long periods.

One can conclude that the blocks of folded chains broken in the initial iPP morphology are subjected to such a high concentration of deformational energy that they melt and reorganize according to the temperature of drawing, like in polyethylene.[57] The resultant long period is more characteristic of the drawing temperature than the initial state of the iPP sample. The change of long period is abrupt, indicating a discontinuous step in the transformation form the original microspherulitic into the fiber structure.[55]

Correlation between ^{1}H Transverse Relaxation Rate and the Domain Thickness of the Rigid Domains

The morphology of semi-crystalline polymers and domain thickness characterize the material on a scale ranging from nanometers to hundreds of nanometers and micrometers. Analysis of the chain dynamics, revealed inter alia by the ^{1}H transverse magnetization rate, is a useful tool for a better understanding of the microscopic properties of heterogeneous polymers.

The value of the ^{1}H effective transverse magnetization relaxation rate ($1/T_2^{rigid}$) for the rigid domains is related to the type and frequency of chain motions, and to intrachain and interchain interactions in those domains. A faster transverse relaxation rate corresponds to an increase in the dipolar coupling due to denser chain packing and/or better crystal organization that could affect chain mobility in rigid domains.

The correlation between $1/T_2^{rigid}$ and domain thickness d_r for different draw ratios and drawing temperatures is shown in Figure 12. For iPP samples uniaxially stretched at 25 °C, the increase in $1/T_2^{rigid}$ and decrease in d_r with increasing drawing ratio are due to the immobility of the polymer chains and the fragmentation of the crystalline blocks. At this drawing temperature, the chain mobility is

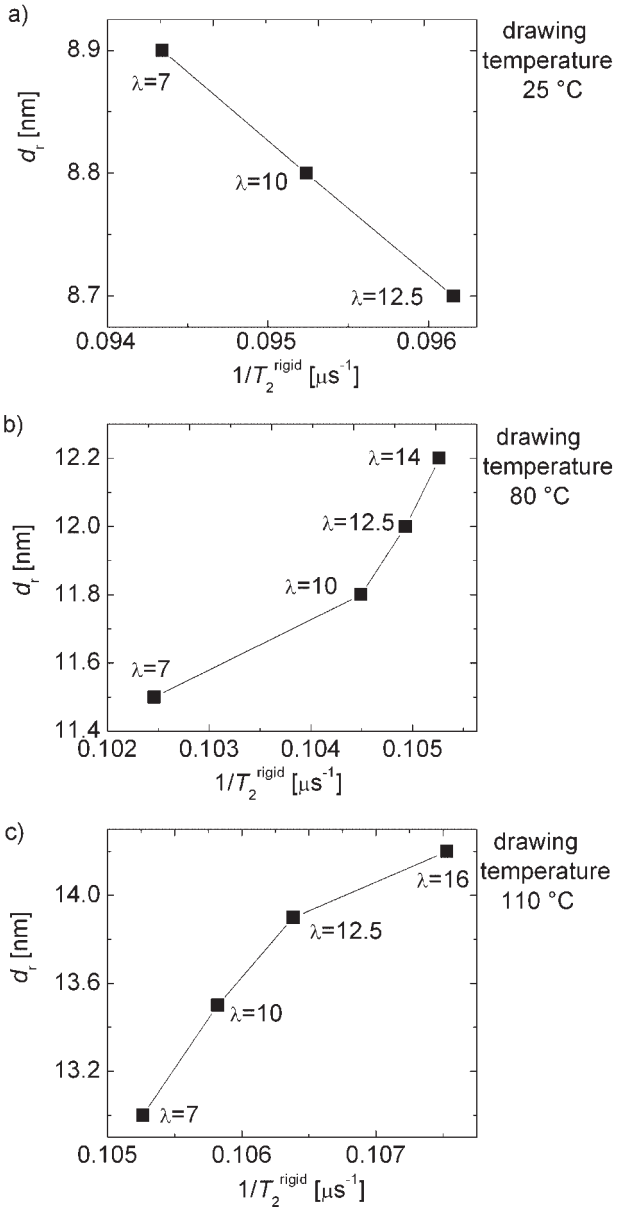

Figure 12. Correlation of the thickness of the rigid domains with the ^{1}H transverse magnetization relaxation rate of the rigid domains ($1/T_2^{rigid}$) for iPP that was uniaxially draw at 25 (a), 80 (b) and 110 °C (c) with 10 mm · min^{-1}.

lower and the reorganization of the morphology from spherulitic to fibrillar is limited. The increase in the values of $1/T_2^{rigid}$ and d_r, for iPP samples uniaxially stretched at 80 and 110 °C, are due to a decrease in chain mobility. Moreover, at this deformation temperature the chain mobility is larger compared with the deformation temperature of 25 °C, which facilitates the reorganization of the morphology. The perfection of the crystals can occur during the strain-induced recrystallization process and/or immobilization of the soft phase, which both occur at higher deformation temperatures.

We note that all NMR measurements were done at 70 °C on stretched iPP samples recovered after strain. Therefore, the dependences shown in Figure 12 reflect changes in the thickness and chain reorganization of crystals due to irreversible iPP deformation at different temperatures. Elastic recovery in the soft phase can cause some changes in the phase composition, domain sizes and molecular mobility after applied stress is removed. However, these changes would not affect the conclusions about the effect of draw ratio, drawing rate and temperature of structural reorganization during drawing of iPP.

Conclusion

In the present work, we have investigated using ^{1}H solid-state NMR the changes in the phase composition (namely the amounts of rigid fraction/crystallinity, semi-rigid and soft amorphous fractions), chain mobility and domain thickness for uniaxially drawn iPP at different draw ratios, drawing rates and drawing temperatures. Such an extensive NMR study of the changes in the morphology and chain dynamics of deformed iPP under various conditions has not been reported before. Moreover, NMR is a unique analytical method to give information of the modification of the interfacial and amorphous fractions of deformed iPP. The correlation between the microscopic and mesoscopic properties of iPP and the macroscopic deformation can be better established.

The values of the rigid fraction/degree of crystallinity obtained by NMR and IR are in the same order of magnitude. The small difference can be explained by the analysis of NMR and IR data using three- and two- phase models, respectively. An increase in the drawing rate from 1 to 100 mm · min^{-1} does not affect the phase composition and chain mobility of iPP after stretching at 80 °C. The drawing temperature was shown to have a significant effect on the phase composition, chain mobility, long period and lamellar thickness. The results show that the amount of the rigid fraction/crystallinity increases as the draw ratio and drawing temperature increase for the entire range of draw ratios ($\lambda = 1$, 7–16). For example, the amount of the rigid fraction in non-drawn iPP is 55 wt.-% at 70 °C. Its value at the same temperature increases up to 65 wt.-% for iPP stretched to $\lambda = 12.5$. Higher draw ratios and higher drawing temperatures above 80 °C of iPP resulted in an increase in the thickness of lamellae from 11 to 16.5 nm that can be explained by partial melting and recrystallization, as well as immobilization of the soft phase. We can conclude that the phase composition, chain mobility and the thickness of domains largely depend on deformation conditions, namely draw ratio and drawing temperature.

Correlations between the following molecular parameters were established: (1) the amount of the rigid domains and their thickness; (2) chain mobility in the rigid domains and the thickness of these domains. A semi-quantitative model was developed to describe the correlation between the amount of the rigid fraction and the thickness of the crystalline domain in the range of high drawing temperatures. Moreover, the correlation between the long period and the drawing temperature was analyzed based on a phenomenological law applied before on polyethylene.[57] These relationships differ for iPP uniaxially drawn at 25 °C and at higher deformation temperatures $\geq$80 °C. The results reveal the important role of chain mobility during strain-induced transformation of the spherulitic morphology to a fibrillar one. At 25 °C, the rate of molecular motion is not high enough to follow molecular displacements that are caused by the macroscopic strain. This is confirmed by the fact that stress-strain dependence at 25 °C largely depends on the deformation rate. High local forces that cause crystal slip process damage crystalline structures, as can be concluded from a small decrease in the lamellae thickness. At the same time, the amount of the rigid fraction increases due to the immobilization of highly strained chain fragments in the soft phase. Deformation at temperatures of 80 °C and higher is not accompanied by high local forces due to more intensive chain motion. Moreover, a heat release during drawing causes partial melting followed by recrystallization. This results in thicker crystals and larger long periods. As far as chain mobility is concerned, it decreases with increasing draw ratio both in the rigid and soft phases. The decrease is pronounced at higher deformation temperatures, which points out a more perfect structure organization due to partial melting followed by recrystallization at higher deformation temperatures.

Acknowledgements: This study was sponsored by *SABIC Europe BV*. Cristian Hedesiu gratefully acknowledges *SABIC Europe BV* for a PhD grant. The authors are grateful to *Jaap van der Weert* for performing the IR measurements and *Rudy Deblieck* for helpful discussions.

Received: September 28, 2007; Revised: December 1, 2007; Accepted: December 3, 2007; DOI: 10.1002/macp.200700503

DOI: 10.1002/macp.200700503

Keywords: domain sizes; IR spectroscopy; isotactic poly(propylene); mechanical deformation; proton solid-state NMR; spin-diffusion NMR

[1] R. Popli, L. Mandelkern, *J. Polym. Sci., Part B: Polym. Phys.* **1987**, *25*, 441.
[2] J. C. Halpin, J. L. Kardos, *J. Appl. Phys.* **1972**, *43*, 2235.
[3] R. H. Boyd, *Polym. Eng. Sci.* **1979**, *19*, 1010.
[4] R. H. Boyd, *J. Polym. Sci., Part B: Polym. Phys.* **1983**, *21*, 493.
[5] G. Strobl, M. Schneider, *J. Polym. Sci., Part B: Polym. Phys.* **1980**, *18*, 1343.
[6] L. Mandelkern, "*Crystallization of polymers*", McGraw-Hill, New York 1964.
[7] L. Mandelkern, *J. Polym.* **1985**, *17*, 337.
[8] M. Negahban, A. S. Wineman, *Int. J. Eng. Sci.* **1992**, *30*, 819.
[9] F. J. Wortmann, K. V. Schulz, *Polymer* **1996**, *37*, 819.
[10] R. H. Boyd, *Polymer* **1985**, *26*, 323.
[11] R. H. Boyd, *Macromolecules* **1984**, *17*, 903.
[12] A. Bellare, R. E. Cohen, A. S. Argon, *Polymer* **1993**, *34*, 1393.
[13] U. Goschel, K. Deutscher, V. Abetz, *Polymer* **1996**, *37*, 1.
[14] R. Silvestry, P. Sgarzi, *Polymer* **1998**, *39*, 5871.
[15] E. W. Fischer, G. F. Schmidth, *Angew. Chem.* **1962**, *74*, 551.
[16] A. Peterlin, *J. Polym. Sci.* **1967**, *18*, 123.
[17] I. L. Hay, A. Keller, *Kolloid-Z. & Z. Polym.* **1965**, *204*, 43.
[18] A. Peterlin, *Kolloid-Z. & Z. Polym.* **1967**, *216/217*, 129.
[19] A. Peterlin, *Polym. Eng. Sci.* **1969**, *9*, 172.
[20] E. W. Fischer, M. Goddar, *J. Polym. Sci.* **1969**, *C16*, 4405.
[21] R. S. Stein, *Polym. Eng. Sci.* **1969**, *9*, 320.
[22] P. J. Flory, D. Y. Yoon, *Nature* **1978**, *272*, 226.
[23] A. Peterlin, *J. Mater. Sci.* **1971**, *6*, 490.
[24] J. X. Li, W. L. Cheung, C. M. Chan, *Polymer* **1999**, *40*, 2089.
[25] L. Lin, A. S. Argon, *J. Mater. Sci.* **1974**, *9*, 2034.
[26] X. C. Zhang, M. F. Butler, R. E. Cameron, *Polymer* **2000**, *41*, 3797.
[27] J. M. Brady, E. L. Thomas, *Polymer Prep.* **1986**, *27*, 1.
[28] A. Peterlin, *Appl. Polym. Symp.* **1973**, *20*, 269.
[29] A. Peterlin, *Colloid Polym. Sci.* **1987**, *265*, 357.
[30] K. Schmidt-Rohr, H. W. Spiess, "*Multidimensional Solid-state NMR and Polymers*", Academic Press, London 1994.
[31] K. Schmidt-Rohr, H. W. Spiess, *Macromolecules* **1991**, *24*, 5288.
[32] E. Günther, B. Blümich, H. W. Spiess, *Macromolecules* **1992**, *25*, 3315.
[33] A. Kivinen, M. Ovaska, K. Soljamo, *Chem. Phys. Lett.* **1986**, *128*, 4.
[34] A. Buda, D. E. Demco, M. Bertmer, B. Blümich, B. Reining, H. Keul, H. Höcker, *Solid State Nucl. Magn. Reson.* **2003**, *24*, 39.
[35] Y. Ba, J. A. Ripmesster, *J. Chem. Phys.* **1998**, *108*, 8589.
[36] B. R. Cherry, C. H. Fujimito, C. J. Cornelius, T. M. Alam, *Macromolecules* **2005**, *38*, 1201.
[37] M. Goldman, L. Shen, *Phys. Rev.* **1961**, *144*, 321.
[38] D. E. Demco, A. Johansson, J. Tegenfeldt, *Solid Nucl. Magn. Reson.* **1996**, *7*, 17.
[39] W. Heinsen, *J. Polym. Sci.* **1959**, *38*, 134.
[40] R. J. Samuels, *Makromol. Chem.* **1981**, *4*, 241.
[41] Y. V. Kissin, *J. Polym. Sci.: Polym. Phys. Ed.* **1983**, *31*, 2085.
[42] R. Mendoza, G. Regnifer, W. Seiler, J. L. Lebrun, *Polymer* **2003**, *44*, 3363.
[43] P. Zhu, E. Graham, *Polymer* **2004**, *45*, 2603.
[44] W. Wenig, F. Herzog, *J. Appl. Polym. Sci.* **1993**, *50*, 2163.
[45] P. Zhu, J. Tung, G. Edward, *Polymer* **2005**, *46*, 10960.
[46] K. Mezghani, R. A. Cambell, P. J. Phillips, *Macromolecules* **1994**, *27*, 997.
[47] F. Auriemma, C. De Rosa, T. Boscato, P. Corradini, *Macromolecules* **2001**, *34*, 4815.
[48] K. Yamada, S. Matsumoto, K. Tagashira, M. Hikosaka, *Polymer* **1998**, *39*, 5327.
[49] J. J. Zhou, J. G. Liu, S. K. Yan, J. Y. Dong, L. Li, C. M. Chan, J. Schultz, *Polymer* **2005**, *46*, 4077.
[50] C. Hedesiu, D. E. Demco, R. Kleppinger, B. Blumich, K. Remerie, V. M. Litvinov, *Polymer* **2007**, *48*, 763.
[51] A. Abragam, "*The Principles of Nuclear Magnetism*", Clarendon Press, Oxford 1961.
[52] C. Hedesiu, D. E. Demco, R. Kleppinger, G. Vanden Poel, W. Gijsbers, B. Blümich, K. Remerie, V. M. Litvinov, *Macromolecules* **2007**, *40*, 3977.
[53] W.-G. Hu, K. Schmidt-Rohr, *Polymer* **2000**, *41*, 2979.
[54] E. W. Fisher, G. F. Schmidt, *Angew. Chem.* **1962**, *74*, 551.
[55] F. J. Baltá-Calleja, A. Peterlin, *J. Mater. Sci.* **1969**, *4*, 722.
[56] A. Peterlin, C. Reinhold, *J. Polym. Sci., Part A: Polym. Chem.* **1965**, *3*, 2801.
[57] R. Corneliussen, A. Peterlin, *Makromol. Chem.* **1967**, *105*, 193.